

# Mechanical testing of titanium/aluminium–silicon interfaces by push-out

Olivier Dezellus · Lucile Milani · Françoise Bosselet ·  
Myriam Sacerdote-Peronnet · Dominique Rouby ·  
Jean-Claude Viala

Received: 24 July 2007 / Accepted: 17 December 2007 / Published online: 18 January 2008  
© Springer Science+Business Media, LLC 2008

**Abstract** Mechanical properties of Ti/Al–7Si assemblies produced by insert moulding were studied with a classical push-out test and a variant that is the circular-bending test. Special care has been taken for controlling both the reactivity at the Ti/Al–7Si interface and the metallurgical health of the Al–7Si matrix. Mechanical tests until complete debonding have been completed with interrupted tests, metallographic characterizations and FEM analysis of elastic stress state. A mean shear strength of the interface of about 120 MPa was obtained. When the Ti insert is solely fretted in the matrix, without chemical interaction between Ti and the Al–7Si alloy, the mean shear strength is significantly lower (48 MPa). This result clearly shows that chemical interaction at the interface (formation of a thin TiSi layer at the Ti side and a thick Al<sub>3</sub>Ti(Si) layer at the Al–7Si alloy side) improves the mechanical properties of the assembly. It is also shown that the failure sequence is characterized both by crack propagation from bottom to top and matrix yielding from top to bottom. Actually, interface damaging begins by crack initiation at the specimen bottom face (not at the top face and under the indenter) in a nearly pure mode I sollicitation at a radial tensile stress of about 100 MPa.

## Introduction

Among the different ways used for processing high performance structural mechanical parts, joining of materials with complementary properties is of particular interest. For example it is possible to locally enhance stiffness and toughness of classical aluminium castings for aeronautical or automotive components with titanium or titanium alloys inserts [1, 2]. When using conventional die casting procedure, the insert is simply embedded in the light alloy and oxide layers (iron oxide on one side and aluminium on the other) prevent a direct contact from being established. As a consequence, no real interfacial bond exists and the insert has to be designed with complex shape (as cogwheel for example) to ensure mechanical anchoring of the two parts. However, because of that shape, stresses are not uniformly distributed along the interface and, for instance, when clamping pressure exerted by the light alloy upon cooling vanished, some cavities up to a few hundreds of micron wide might appear. Existence of these flaws limits both the air or water tightness of the assembly and its mechanical resistance [3]. Finally, insertion of stiff metals like titanium or iron in light alloys castings (aluminium or magnesium alloys) requires the formation of a sound metallurgical bond between the two metals at the insert/alloy interface to improve the functionality of the whole assembly [4, 5]. Thereafter, it is important to characterize the mechanical properties of the resulting multimaterial. This article deals with the mechanical characterization of bimetallic samples with a well known, characterized and controlled interface. As no ASTM test exists for such assemblies, push-out testing was chosen to investigate their mechanical strength. Combining push-out test results with characterization of the interfacial zone (by Optical Microscopy, Scanning Electron Microscopy—SEM—and Electron Micropobe

---

O. Dezellus (✉) · L. Milani · F. Bosselet ·  
M. Sacerdote-Peronnet · J.-C. Viala  
Université Claude Bernard Lyon 1, LMI – UMR CNRS No  
5615, 43 Bd du 11 novembre 1918, 69622 Villeurbanne Cedex,  
France  
e-mail: olivier.dezellus@univ-lyon1.fr

D. Rouby  
INSA-Lyon, GEMPPM – UMR CNRS No 5510, 20 av. Albert  
Einstein, 69621 Villeurbanne Cedex, France

Analyses—EPMA) and with numerical analysis of the stress state has led us to propose a failure mode for the titanium/light weight aluminium alloy assembly.

## Experimental

### Materials and processing

Bimetallic samples were processed from an Al–7 wt%Si–0.3 wt%Mg casting alloy (provided by Alcan<sup>®</sup>), and referred as A356.2 according to ASTM standards (referred as AS-7 in this article). The alloy composition is given in Table 1. Inserts rods were made of pure titanium provided by Goodfellow<sup>®</sup> (composition in ppm: Al 500, Co 2, Cr 500, Cu 200, Fe 300, Mg 20, Mn 500, Ni 500, Si 200, Sn 200, Ta 10, V 500 and Ti balance). The titanium rods (5 mm in diameter) all received the same surface preparation by mechanical abrasion leading to a mean surface roughness of about 3  $\mu\text{m}$ . Moreover, just prior to insertion, titanium and aluminium alloy pieces were degreased in an ultrasonic bath of dichloromethane.

The AS-7 pieces were melted in a baked stumatite crucible heated by Radio-Frequency (RF) coupling. Before immersion of the Ti rod the bath was regularly stirred (during a few hours) and the surface oxide skin removed. The bottom of the crucible was machined and a device put on its top so that the titanium insert was perfectly vertical and centred (see [6] for more details on the experimental apparatus). The dipping temperature was measured with a precision better than 0.2  $^{\circ}\text{C}$  by plunging in the melt a K-type (Ni/Cr) thermoelectric couple. Note that with a bath

heated at 720  $^{\circ}\text{C}$ , firstly a temperature decrease of about 20–30  $^{\circ}\text{C}$  is observed upon Ti rod dipping, next temperature is stabilized at about  $700 \pm 4$   $^{\circ}\text{C}$  after 1 min of immersion. In the following, the experimental temperature is systematically referred to the stabilized value.

If the solidification is not controlled, many shrinkage voids can appear either at the interface for unbonded zone or in the bulk of the matrix. In both cases, presence of these voids has a detrimental effect on the mechanical characteristics of the bimetallic assembly [7]. Therefore, an attempt has been made to enhance the metallurgical health of both the interface and the matrix by processing a kind of directional solidification. For that purpose, induction coils were displaced from the middle to the lower part of the crucible in order to establish a thermal gradient through the liquid bath. After 10 min under such conditions, RF power supply was turned off and the aluminium alloy was allowed to cool and solidify around the insert.

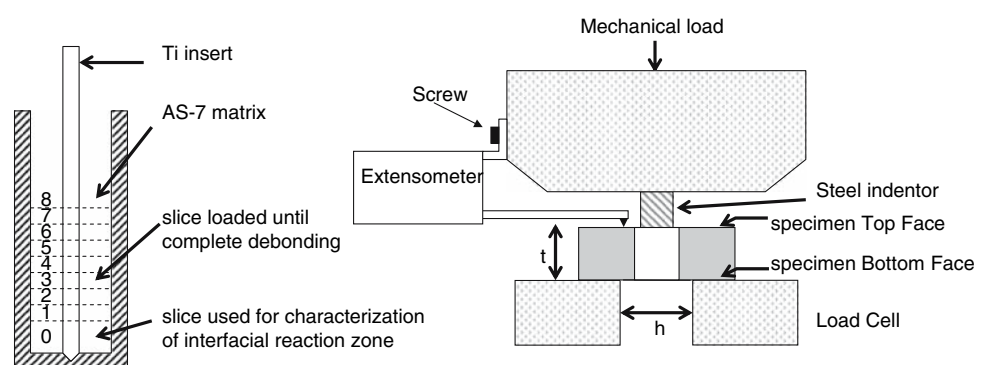
### Push-out procedure

After solidification, the bimetallic samples were cut by Electron Discharge Machining (EDM) into slices with a thickness  $t$  of 5 mm, the cross section of these slices being perpendicular to the rod axis. End sections of each cylinder were diamond polished to a finish better than 1  $\mu\text{m}$  for examination by optical microscopy (OM), scanning electron microscopy (SEM) and electron probe microanalysis (EPMA). Other slices were used for two types of push-out testing: (i) classical tests as shown in Fig. 1, (ii) and a variation named circular bending performed with an

**Table 1** Composition (wt%) of the AlSi7Mg0.3 alloy provided by Alcan<sup>®</sup>

Element	Si	Fe	Cu	Mn	Mg	Ni	Zn	Pb + Sn	Sb	Ti	Others
Min.	6.7				0.3						
Max.	7.3	0.14	0.02	0.04	0.4	0.02	0.04	0.02	0.16	0.15	0.1
$\pm$	0.2	0.01	0.01	0.01	0.02	0.01	0.01	0.01	0.02	0.01	

**Fig. 1** Scheme of bimetallic sample, slices references and principle of the pushout test



enlarged indenter and support hole. The tests were performed by using an INSTRON 1195 testing frame equipped with a compression load cell of 100 kN capacity. The insert was put on a plate with a circular support hole of 6 mm diameter (22 mm for circular bending) and pushed by means of a flat-bottomed STUB steel (ball bearing steel) cylinder, concentric with the support hole, with a 4 mm diameter, i.e. 80% of the titanium insert diameter (8 mm for circular bending, i.e. 160% of the insert diameter). It should be noted that this results in ratios of specimen thickness ( $t$ ) to hole size ( $h$ ) of  $t/h = 0.83$  and  $t/h = 0.22$  for classical push-out and circular bending, respectively. The cross-head displacement rate was of  $0.2 \text{ mm min}^{-1}$ . The relative displacement of the indenter compared to the AS-7 matrix was measured by using a modified extensometer (see Fig. 1). This experimental device makes it possible to remove the influence of the machine compliance on the displacement measurements, therefore, only the compliance of the indenter remains. Finally, for some samples, acoustic emission was also recorded in order to more clearly identify the debond event and to follow the damage. After mechanical loading, slices were embedded in resin and cut with a diamond wire to prepare a polished vertical section, i.e. parallel to the axis of the insert.

#### Analytical procedure

In order to describe the stress distribution in a bimetallic slice during push-out test at different load level, Finite Element Modeling (FEM) was performed. Due to axis symmetry, two-dimensional finite element meshes were generated by the RDM 6.16<sup>®</sup> software. The mesh was built by using the Delaunay triangulation method with 6 nodes triangles. The whole geometry is modelled: a titanium insert, surrounded by an AS-7 matrix, lying on a steel support with a drilled hole and under a STUB indenter tool (ball bearing steel) mounted in a support piece made in steel. The element size was decreased in the vicinity of the Ti/AS-7 interface, the top and the bottom faces, in order to refine the mesh where most of stress variations were expected. The effect of the flat bottom indenter was modeled as a uniform pressure on the top face of the support piece. Note that the thermal residual stress state is not taken into account in the present study. Actually, cutting of the 5-mm slices for push-out tests alters shear stress along the  $z$ -axis (vertical) due to introduction of free surfaces perpendicular to the cylinder axis. This effect is difficult to evaluate and therefore good description of the residual thermal stresses remaining in the tested slices is difficult [8]. The solidification process used in the present study leads to nearly directionally solidified aluminium alloys, without

shrinkage voids. Under such cooling conditions fretting stresses are maximized. Therefore, for an experimental study of the effect of fretting stresses, a specific assembly has been made to prevent chemical interaction between titanium and AS-7 alloy (by oxidizing the titanium rod before insertion in the AS-7 bath) and to compare the mechanical behaviour of bimetallic assemblies only fretted and chemically bonded.

#### Classical Push-out testing

##### Interface chemistry

The reaction zone formed at the Ti/AS-7 alloy interface during the insertion process appeared to be similar to those previously observed and characterized in our laboratory at the surface of titanium plates after dipping in the same AS-7 alloy at about the same temperature [9]. The reaction zone shown in Fig. 2 mainly consists of crystals of the intermetallic compound  $\text{Al}_3\text{Ti}$  (tetragonal,  $I4/mmm$ ) [10] with a typical size of  $10 \mu\text{m}$ . This compound was unambiguously characterized by X-ray diffraction (Cu- $K_\alpha$  radiation) at the surface of a Ti plate that was dipped for 15 min in the AS-7 alloy at  $730 \text{ }^\circ\text{C}$ , water quenched and chemically attacked in a NaOH solution to remove the solidified alloy (Fig. 2). According to EPMA results, the actual chemical composition in at% of the  $\text{Al}_3\text{Ti}$  crystals constituting the outer layer in Fig. 2 is Al:Si:Ti = 63:12:25. This is consistent with a substitution of Al atoms by Si atoms in the structure of the intermetallic compound that can be designated as  $\text{Al}_3\text{Ti}(\text{Si})$  or more precisely  $(\text{Al}_{1-x}\text{Si}_x)_3\text{Ti}$ , as previously reported in [11]. A sub-micronic layer can moreover be distinguished

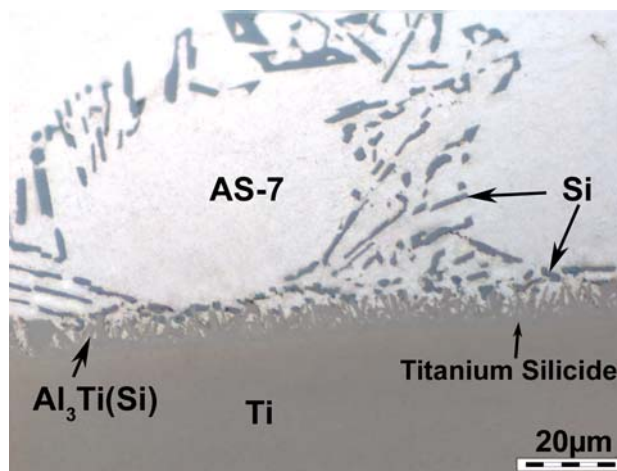


**Fig. 2** Optical micrograph of interfacial reaction zone between Ti and an AS-7 alloy obtained after 15 min at  $700 \text{ }^\circ\text{C}$  and a directional solidification process. Section perpendicular to the Ti rod axis

between  $\text{Al}_3\text{Ti}$  and Ti in Fig. 2. This submicronic layer contains titanium silicides; and more especially indications were obtained for the presence of TiSi [9].

### Load versus displacement curves

The typical load–displacement response for an AS-7 matrix reinforced with a Ti insert in the case of a 5-mm thick slice is reported in Fig. 3.

A pre-load (6 daN) is applied to the insert to allow an easier setting up of the acoustic emission device. Therefore the first load rise is not visible on Fig. 3. Mechanical fitting being quasistatic, the first loading stage (from  $\Delta l = 0$  mm to  $\Delta l = 0.01$  mm) consists in compensating misalignments and is therefore characterized by a gentle increase of the load. The first acoustic emission event occurs at a critical load value equal to  $F_C = 600$  daN (67% of the maximum load value). It is interesting to note that before  $F_C$ , a linear regression performed on the  $F$  versus  $\Delta l$  curve leads to a correlation coefficient of 0.99 that remains higher than 0.97 until the load has reach a value of 700 daN. Therefore, the end of a quasi-linear stage could not be used to clearly identify the end of elastic loading  $F_C$  and the beginning of interface damaging. Moreover, acoustic emission appears to be a useful tool to determine the critical load value  $F_C$ . From  $F = F_C$  to the maximum value  $F_{\text{Max}} = 891$  daN ( $\Delta l_{\text{Max}} = 0.19$  mm) deviation to the linearity obviously occurs corresponding to a stable insert displacement under increasing load. In parallel the number of acoustic emission events increases continuously. Once the maximum value is attained, the load is observed to decrease gently (no load drop is observed) to a friction load. Note that no acoustic emission event is associated with sliding of the insert. Figure 4 shows push-out load versus displacement curves for a series of slices belonging to different bimetallic assemblies. The results appear to be quite reproducible not

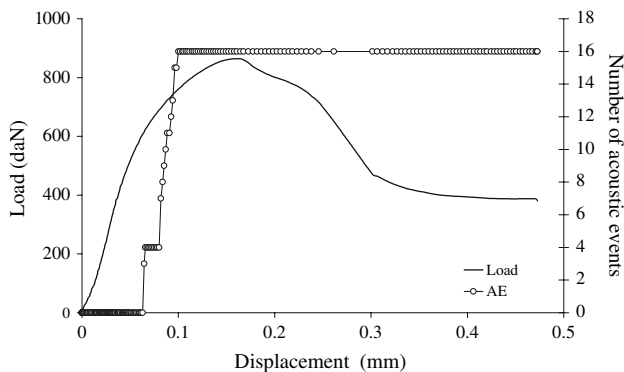


**Fig. 3** Typical load–displacement curve obtained by push-out testing for an AS-7 matrix reinforced with a titanium insert in the case of a 5 mm thick slice

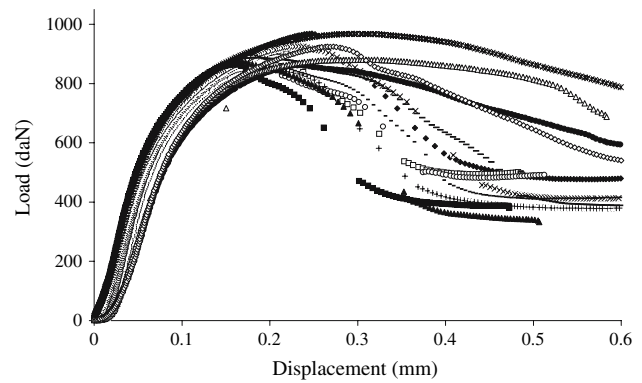


**Fig. 4** Comparison of load–displacement curves obtained by push-out testing for a series of slices belonging to different AS-7 matrix reinforced with titanium inserts in the case of a 5 mm thick slice

only from one slice to another cut along one assembly but also from one casting to another.

### The mean shear stress value

The mean shear stress at the interface (assumed to be constant along the whole length of the insert during sliding in the AS-7 matrix) associated to the applied load value is established from the load  $F$  and the surface area of the insert using the following formula

$$\tau = \frac{F}{\pi \cdot D \cdot t}$$

where  $D$  is the diameter of the insert (5 mm), and  $t$  is the disc thickness (5 mm). The mean shear strength obtained when the maximum load is attained is about 120 MPa. Durrant et al. [2] obtained similar values for steel inserts coated with titanium and attributed them mainly to a high residual radial stress due to CTE mismatch and fretting phenomena during cooling. Finally, they concluded that the bond between titanium and AS-7 alloy was weak. The solidification process used in the present study leads to nearly directionally solidified aluminium alloys, without shrinkage voids. Under such cooling conditions fretting stresses are maximized. The mean value of the maximum load attained for slices belonging to the only fretted assembly (Ti rod had been oxidized before insertion to prevent any intimate contact with the liquid alloy—no  $\text{Al}_3\text{Ti}(\text{Si})$  layer was formed), was 380 daN leading to a mean shear strength of about 48 MPa. Such a value represents 40% of the maximum value obtained when chemical interaction occurs between titanium and AS-7 alloy. Therefore, we conclude that allowing the chemical interaction between Ti and AS-7 enhances the mechanical properties of the assembly indicating that a reacted Ti/AS-7 interface is stronger than an only fretted one.

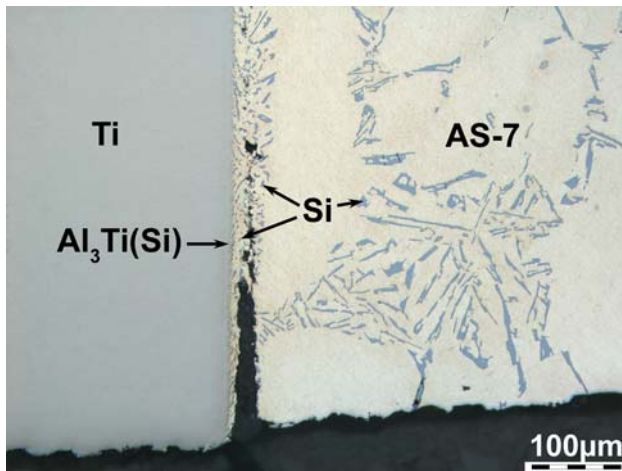


**Fig. 5** Optical micrograph after push-out test interrupted at 60% of the maximum load value—initiation of interfacial cracking at the specimen bottom face

**Damage characterization**

In order to understand the scenario of failure it is necessary to establish the temporal sequence of damaging and the most important point is to determine where failure initiation occurs. Therefore some push-out tests were interrupted after detection of the first acoustic event (at about 60% of the maximum load value). Afterwards, the slices were embedded in a resin, cut with a diamond wire and polished to a finish better than 1 µm to characterize the damage along a vertical section. Optical characterizations indicate crack initiation is observed at the specimen bottom face, either in the intermetallic reaction layer or in the matrix nearby the interface (see Fig. 5).

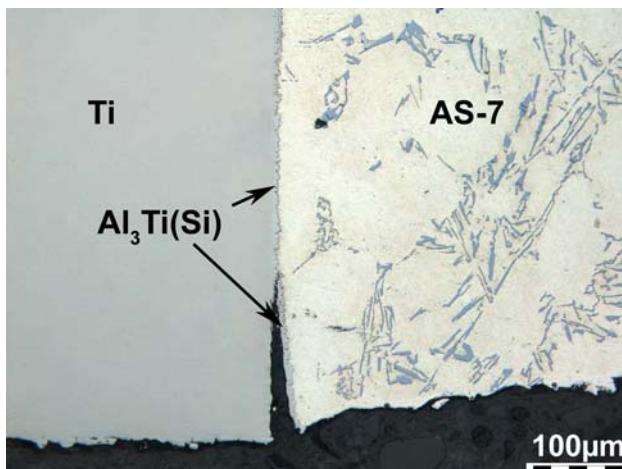


**Fig. 6** Typical optical micrograph of a Ti/AS-7 assembly after mechanical loading and complete failure. Crack initiation in the intermetallic layer and deviation towards the AS-7 matrix

Next, after complete failure, the main features observed on polished vertical section, i.e. parallel to the axis of the insert, for classical push-out testing (summarized in Figs. 6 and 7) are as follows:

- Failure is mainly cohesive and, far away from the specimen bottom face, located in the AS-7 matrix. However, optical characterizations indicate that, in the lower part of the slices, crack has propagated either along Si crystals nearby the interface, or in the intermetallic reaction layer.
- Along the insert, except in the lower part of the assembly, silicon platelets present a preferential orientation (from top to bottom) in a cylinder of matrix with a typical thickness of 100 µm. Moreover, in this matrix cylinder, multiple fractures are observed in the silicon platelets. Combination of these two features clearly indicates permanent plastic shearing of matrix induced by the Ti insert displacement (see Fig. 7).

Note that during propagation towards the top face, crack path is difficult to follow because the crack deviates in the AS-7 matrix and becomes invisible due to sticking of the crack lips under an increasing shear-stress component (see Sect. “Finite element modeling” and Fig. 8).

**Finite element modelling**

The interfacial failure sequence described in the preceding section is in response to the stress state imposed by the indenter load. The development of stress criteria for failure initiation in multimaterials assemblies is presently of main interest [12]. Therefore, the stress state (radial stress  $\sigma_{rr}$ ,

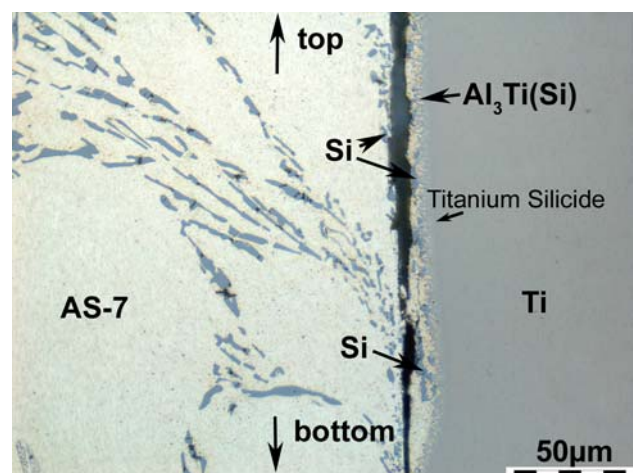


**Fig. 7** Representative optical micrograph of the AS-7 matrix after mechanical loading along the interface. Note that failure progresses along the Si platelets in the matrix nearby the interface. Fractures and preferred orientation of Si platelets indicate permanent plastic shearing of the matrix

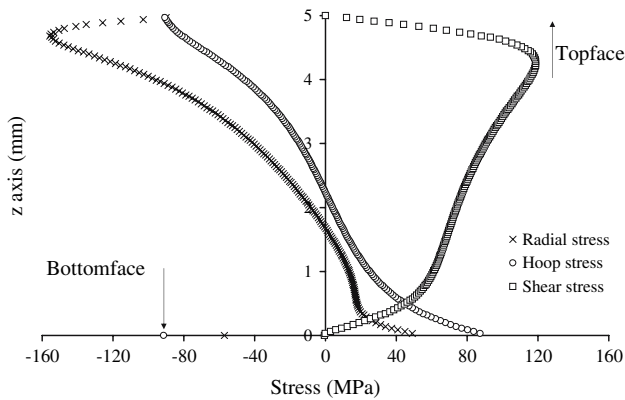


**Fig. 8** Evolution of radial stress  $\sigma_{rr}$ , hoop stress  $\sigma_{\theta\theta}$  and shear stress  $\sigma_{rz}$  along the Ti/AS-7 interface during push-out test at a 600 daN load level (load level of the first acoustic event)

hoop stress  $\sigma_{\theta\theta}$  and shear stress  $\sigma_{rz}$ ) along the Ti/AS-7 interface has been evaluated for an applied load of 600 daN corresponding approximately to the first acoustic event (see Fig. 8).

Several features are noteworthy. First, the difference in diameter between the hole of the supporting piece and the titanium insert induces bending and the appearance of important interfacial radial tension stress at the lower free surface  $\sigma_{rr} = 50$  MPa. The sign of the radial stress changes only at 1.7 mm from the lower free surface. It is therefore concluded that the interface crack that initiate at the specimen bottom face (see Fig. 5), is caused by the large magnitude of radial tension stress. It has been already reported that thin slice geometry used in the present study ( $t/h = 0.83$ ) induces the important bending stress at the specimen bottom face [13]. Note that even without any bending effect the influence of axial residual stresses could also be responsible of bottom face cracking [14, 15]. While initiation of a bottom face crack occurs under almost pure mode I conditions, the large shear stress level at the interface (mean value higher than 70 MPa with a peak at 120 MPa located at 4.3 mm from the lower free surface) suggests that its propagation should occur in an increasingly mode II manner. This raises the likelihood of crack arrest because of the greater crack growth resistance of the interface as the phase angle characterizing the modal mixity increases [16–18]. Moreover, propagation of the crack towards the top face also drives it into an increasingly compressive radial stress field, which suggests that blunting of crack propagation occurs. Concurrent with crack propagation from the specimen bottom face is matrix plasticity by shearing at the specimen topface (see Fig. 7 for experimental evidence). Figure 8 indicates that this results of the large shear  $\sigma_{rz}$  stress in the vicinity of the topface which must increase as the crack grows and the applied load increases from  $F_C$  to  $F_{Max}$ . It should be noted

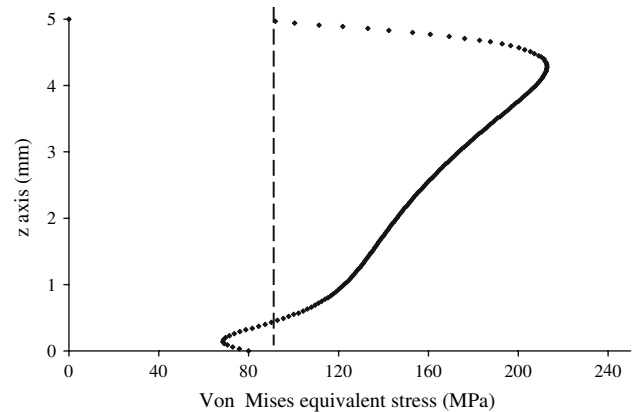


**Fig. 9** Approximate value of the equivalent von Mises stress along the Ti/AS-7 interface under an applied load of 600 daN (first acoustic event). Dashed line represents matrix yield stresses of an as cooled AS-7 matrix

here that the calculated stress state does not take into account the presence of a crack.

Figure 9 shows the equivalent von Mises stress ( $\bar{\sigma}$ ) along the Ti/AS-7 interface for an applied load value of 600 daN. The large value of  $\bar{\sigma}$  (larger than the AS-7 yield stress  $\sigma_0 = 90$  MPa) over nearly the full length of insert/matrix interface, due to the thin slice geometry [13], sustains the occurrence of matrix yielding in the failure sequence. Therefore, crack growth from the bottom face is associated with failure of the ligament in the upper part of the slice due to general plasticity.

In order to sum up, experimental results and FEM show that interfacial failure sequence, in the case of classical push-out tests, is characterized by: (i) crack initiation at the specimen bottom face under mainly tensile conditions; (ii) next, crack propagation from bottom to top occurs in an increasing shear stress state and is accompanied by crack deviation towards the AS-7 matrix; (iii) failure in the upper part of the bimetallic assembly is due to plastic deformation of the matrix under large shear stresses. This result is in contrast with failure mechanism usually assumed for push-out experiments in brittle-matrix composites [19–21] but in agreement with previous results obtained with metallic matrix composites (MMC's) or intermetallic matrix composites (IMC's) with high interfacial toughness [13, 15, 22].

### Circular bending testing

It appears from classical push-out results that damage initiate at slice's bottom face by interface (or nearby interface) cracking. However, the stress state associated with push-out testing is complex in the vicinity of the bottom face due to combination of tensile and shear

stresses. Therefore, some slices have been tested using a different geometry (circular bending) characterized by a nearly pure solicitation mode at the specimen bottom face, where crack initiation occurs. Actually, it appears in Fig. 10 that the stress distribution along the interface in the case of circular bending tests is almost purely tensile at the bottom face and becomes mainly compressive at the top face (note that singularities for radial stress at the specimen top and bottom faces make calculations difficult with the software used). The intensity of the two other stresses (hoop stress  $\sigma_{\theta\theta}$  and shear stress  $\sigma_{rz}$ ) along the interface is significantly lowered compared to the classical push-out testing (by a factor 2). Finally, it can be concluded that solicitation mode associated to circular bending test is closer to a pure mode I than for classical push-out test.

The typical load–displacement response for an AS-7 matrix reinforced with a Ti insert (5 mm thick slice) tested with the circular bending geometry is reported in Fig. 11. The first acoustic event is detected at a critical load value

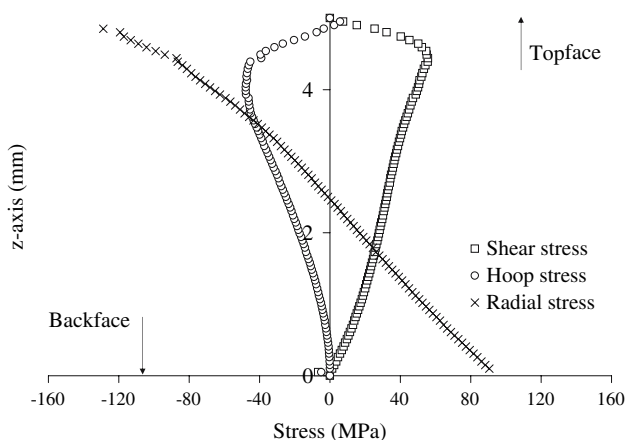


**Fig. 10** Evolution of radial stress  $\sigma_{rr}$ , hoop stress  $\sigma_{\theta\theta}$  and shear stress  $\sigma_{rz}$  along the Ti/AS-7 interface during circular bending test at a 240 daN load level (after detection of the first acoustic event). For comparison, scaling of x-axis is the same as in Fig. 8

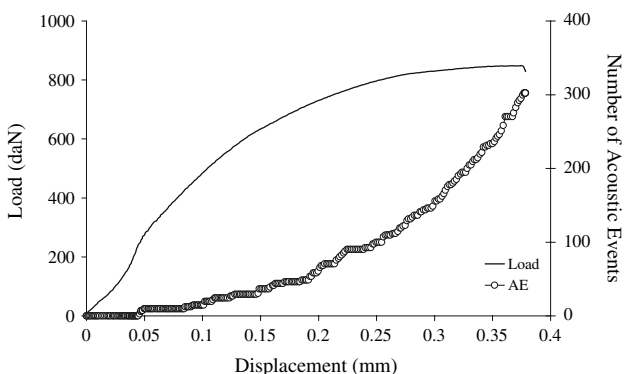


**Fig. 11** Typical load–displacement curve obtained by circular bending testing for an AS-7 matrix reinforced with a titanium insert in the case of a 5 mm thick slice

of about 240 daN, next the load and the number of events increase continuously until the experiment is stopped.

Optical characterizations on slices tested with the circular bending geometry are typical of a nearly pure mode I solicitation. Bending of the specimen and opening of a circular crack at the bottom face are clearly visible to the naked eye. Crack path is similar to the one obtained for classical push-out: either at the intermetallic/matrix interface or in the intermetallic at the specimen bottom face and fully cohesive along the main part of the interface (in the matrix but in the vicinity of the interface). However, due to the most important bending effect, crack propagates under a nearly pure opening mode, with a shear contribution that is minimized. Propagation is also characterized by lower stress intensities (especially for shear stresses) and finally by the absence of general plasticity (according to the von Mises criterion).

In order to sum up, circular bending tests indicate that under almost purely mode I solicitation, crack initiation occurs at the bottom face of Ti/AS-7 assemblies (in the intermetallic reaction layer or nearby the interface) at a load level of about 240 daN corresponding to a tensile stress at the interface of about 90 MPa. Nowadays, the determination of criteria for crack initiation and propagation at interface among different materials is an increasingly important subject not only from basic science viewpoint but also for designing office. Recently, Leguillon has proposed a singular criterion for crack initiation [12, 23] and the value of crack initiation obtained in this study for Ti/AS-7 assemblies under a complex but characterized solicitation mode could be interesting to validate and to sharpen such numerical models.

### Conclusion

Bimetallic specimen test pieces of an AS-7 matrix locally reinforced with a titanium insert that have been produced using an experimental procedure allowing the control of both the interfacial reaction layer and the metallurgical health of the matrix (directional solidification). The results obtain under push-out solicitation highlight the potential of the joining process for producing castings with high mechanical performances. When a chemical bond is established at the Ti/AS-7 interface an important rise of mechanical properties for the bimetallic assembly is observed: the mean shear strength value is about 120 MPa whereas it is of 48 MPa for simply fretted specimens.

A three steps failure sequence is proposed: (i) due to bending effect, crack initiation occurs at the specimen bottom face under tensile stress; either in the intermetallic or in the AS-7 matrix nearby the interface and more precisely along Si platelets. (ii) In a second step, propagation

of the crack towards the top face occurs in an increasingly mode II manner leading to crack deviation from the interfacial area to the bulk of the AS-7 matrix. (iii) Finally, the large value of equivalent von Mises Stress, exceeding the AS-7 yield stress, sustains the occurrence of matrix yielding in the failure sequence. Therefore the failure sequence is both characterized by crack propagation from bottom to top and matrix yielding from top to bottom.

Finally, it has been shown that under nearly pure mode I solicitation, crack initiation at a Ti/AS-7 interface occurs at a load level (240 daN) corresponding to an interfacial tensile stress of about 90 MPa. This value should be useful to validate and sharpen numerical models recently developed to predict crack initiation at interface among dissimilar materials using a singular criterion [12, 23].

## References

1. Clyne TW, Whithers PJ (1993) An introduction to metal matrix composites. Cambridge University Press, Cambridge
2. Durrant G, Gallernault B, Cantor B (1996) *J Mater Sci* 31:589
3. Viala JC, Peronnet M, Barbeau F, Bosselet F, Bouix J (2002) *Compos Part A* 33A:1417
4. Viala JC, Peillon N, Bosselet F, Bouix J (1997) *Mater Sci Eng A* 229A:95
5. Barbeau F, Peronnet M, Bosselet F, Viala JC, Paty F, Loussault JG (2001) French Patent Application N°2 803 783, July 7, 2001, European Patent N°1 118 457, July 25, 2001
6. Dezellus O, Digonnet B, Sacerdote-Peronnet M, Bosselet F, Rouby D, Viala JC (2007) *Int J Adhes Adhes* 27:417
7. Sacerdote-Peronnet M, Guiot E, Bosselet F, Dezellus O, Rouby D, Viala JC (2007) *Mater Sci Eng A* 445–446A:296
8. Redston GD, Stanworth JE (1946) *J Soc Glass Technol* 30:201
9. Peronnet M, Barbeau F, Bosselet F, Viala JC, Bouix J (1999) *J Phys IV* 9:Pr4/223
10. Norby P, Christensen AN (1986) *Acta Chem Scand Ser A* 40A:157
11. Shob O, Nowotny H, Benezovsky F (1962) *Plansee Pulvermet* 10:67
12. Leguillon D (2001) *C R Acad Sci Paris* 329:97
13. Kallas MN, Koss DA, Hahn HT, Hellmann JR (1992) *J Mater Sci* 27:3821
14. Galbraith JM, Rhyne EP, Koss DA, Hellmann JR (1996) *Scripta Mater* 35:543
15. Majumdar BS, Miracle DB (1996) *Key Eng Mater* 116–117:153
16. Evans AG, Ruhle M, Dalgleish BJ, Charalambides PG (1990) *Metall Trans A* 21A:2419
17. Cao HC, Evans AG (1989) *Mech Mater* 7:295
18. O'Dowd NP, Stout MG, Shih CF (1992) *Phil Mag A* 66A:1037
19. Chandra N, Ghonem H (2001) *Compos Part A* 32A:575
20. Kerans RJ (1991) *J Am Ceram Soc* 74:1585
21. Marshal DB (1992) *Acta Metall Mat* 40:427
22. Koss DA, Petrich RR, Kallas MN, Hellmann JR (1994) *Compos Sci Technol* 51:27
23. Brillet-Rouxel H, Arfan E, Leguillon D, Dupeux M, Braccini M, Orain S (2006) *Microelectron Eng* 83:2297